

Article

Study on the Law of Diesel Oil Carrying Water in Lanzhou–Chengdu–Chongqing Product Oil Pipeline Based on Large Eddy Simulation

Tao Zhang , Bin Chen , Kun Sun and Wenjie Chang

Petroleum Engineering School, Southwest Petroleum University, Chengdu 610500, China; 201821000774@stu.swpu.edu.cn (B.C.); 201821000526@stu.swpu.edu.cn (K.S.); changwjz@163.com (W.C.)

* Correspondence: zhangt@swpu.edu.cn; Tel.: +86-139-8229-1124

Received: 12 August 2020; Accepted: 24 August 2020; Published: 27 August 2020



Abstract: Water accumulation at the bottom of the product oil pipeline will lead to corrosion damage to the pipeline. The study on water carrying laws of refined oil could provide a reference for the safe operation of the pipeline. In this paper, the actual size of Lanzhou–Jiangyou section of Lanzhou–Chengdu–Chongqing pipeline was taken as the pipeline size. The volume of fluid (VOF) model of oil-water two-phase flow based on large eddy simulation (LES) was established. The numerical simulation of the water-carrying behavior of the product oil in the inclined pipeline was carried out. The LES-based two-phase flow model can capture the characteristics of stratified flow, wavy stratified flow, and dispersed flow under various operating conditions. The model was applied to simulate the water carrying process under various oil inlet velocities and the inclined pipe angles. The results show that as the pipeline inclined angle is $10\sim 20^\circ$ and the oil inlet velocity is 0.66 m/s, the flow patterns in the pipeline mainly include stratified flow and wavy stratified flow. As the oil inlet velocity is 0.88–1.55 m/s, the flow patterns in the pipe are mainly stratified flow, wavy stratified flow, and dispersed flow. As the inclined angle of the pipeline is $30\sim 40^\circ$, the flow patterns in the pipeline mainly include stratified flows, wavy stratified flows, and dispersed flows. Finally, with the increase of flow time, water can be carried completely from the pipeline through the oil. With the increase of oil inlet velocity, the water carrying capacity of oil gradually increases. With the increase of pipeline inclination, the water carrying capacity of oil firstly increases and then decreases.

Keywords: Lanzhou–Chengdu–Chongqing product oil pipeline; water carrying capacity of oil; VOF; LES; flow pattern

1. Introduction

Lanzhou–Chengdu–Chongqing (Lan–Cheng–Yu) product oil pipeline is a typical pipeline with many ups and downs and large drops with complex terrain [1–3]. The pipeline is put into production by water combined transport. During the production process, due to the large fluctuation of the pipeline, part of the water phase may not be able to climb over the high point, and the water accumulates in the low-lying area along the inclined pipe and forms water in the pipe. Sulfur in the product oil dissolves in accumulated water to form an acidic environment and impurities such as O_2 , CO_2 , $CaCO_3$, and SiO_2 in the pipe form electrochemical internal corrosion in this environment [4,5]. Corrosion of product oil pipeline occurs from time to time and corrosion products do exist in the pigging process of Lan–Cheng–Yu product oil pipeline. Up to now, accidents caused by corrosion products in the product oil pipeline have occurred frequently [6,7]. Since the refined oil pipeline has a certain carrying effect on the water when transporting oil, if the water in the low-lying part of the pipeline can be carried out by oil flow, the corrosion problem caused by the water in the pipeline can be solved [8,9].

The water-carrying process of oil flow in the product oil pipeline is affected by many factors, such as the apparent velocity of oil phase [10,11], physical properties of oil products [12,13], pipeline inclined angle [14,15], accumulated water amount [16], and pipeline diameter [17,18]. It can also be observed through experiments [19,20], numerical simulation [21,22], and theoretical analysis [23]. Based on the above influencing factors, different researchers have studied the influence of water accumulation on pipeline corrosion, interface distribution [24,25], influencing factors of oil flow carrying capacity [26,27], flow pattern characteristics [19,28], and oil-water interface fluctuation characteristics, etc. [14] However, the turbulence models based on Reynolds average method are mostly used in the above simulation studies, which cannot identify the small-scale turbulence information. After average processing, the instantaneous information representing turbulence pulsation is smoothed out, which makes the oil-water interface in the pipeline evenly distributed without any mixing phenomenon. Only stratified flows with the smooth oil-water interface can be identified. Tao Zhang et al. [29] established a multiphase flow model based on the LES method through mutual verification of simulation and experiment. Compared with Reynolds average method, this method adopts the modeling method for small-scale pulsation and direct simulation methods for large-scale pulsation, which shows more flow information. However, all the above studies were carried out under the experimental scale, and the experimental pipe diameter is small, which is quite different from the engineering pipe diameter.

Therefore, a VOF model based on LES was applied to study the laws of diesel oil carrying water in the engineering pipe. The actual size of Lanzhou–Jiangyou section of Lan–Cheng–Yu pipeline was taken as the model size to study the oil carrying water law. All simulation parameters were set strictly according to the actual operating parameters of this section and the numerical calculation method was extended from the experimental scale to engineering practice.

2. Mathematical Model

2.1. Governing Equation of VOF Model

A set of momentum equations is used for different fluid components in VOF. The phase interface of each computing unit can be tracked by introducing the variable of phase volume fraction [30].

Continuity:

$$\frac{\partial u_i}{\partial x_i} = 0 \quad (1)$$

Momentum:

$$\frac{\partial u_i}{\partial t} + \frac{\partial}{\partial x_j} (u_i u_j) = -\frac{1}{\rho} \frac{\partial p}{\partial x_i} + \frac{\partial}{\partial x_j} \left[\nu \left(\frac{\partial u_i}{\partial x_j} + \frac{\partial u_j}{\partial x_i} \right) \right] + g + F_S \quad (2)$$

Volume fraction:

$$\frac{\partial \alpha}{\partial t} + u_i \frac{\partial \alpha}{\partial x_i} = 0 \quad (3)$$

where u_i and u_j are the velocities in i and j directions, m/s; p is pressure, Pa; ρ is density, kg/m³; ν is the kinematic viscosity of the mixture, m²/s; F_S means the unit mass force under surface tension, m/s²; α indicates the dimensionless volume fraction in the liquid phase.

2.2. LES and Sub-Grid Scale Model

Filters are used to deal with the N-S equation in LES. Large-scale vortices are stimulated directly by the unsteady N-S equation. The effects of small vortices on large vortices are modeled through a sub-grid scale (SGS) model [31].

The velocity is divided into the filtered velocity u_i and the sub-grid velocity $u_{i,sgs}$.

$$u_i = \bar{u}_i + u_{i,sgs} \quad (4)$$

A spatial filtering function is used for the filtering process. The filtered N-S equation is shown in Equation (5):

$$\frac{\partial \bar{u}_j}{\partial t} + \rho \bar{u}_i \frac{\partial \bar{u}_j}{\partial x_i} = -\frac{\partial \bar{p}}{\partial x_j} + \frac{\partial}{\partial x_i} \left(\mu \frac{\partial \bar{u}_j}{\partial x_i} - \tau_{ij} \right) \quad (5)$$

where u_i, \bar{u}_j are the filtered velocity in the i and j directions, m/s; t is called time, s; \bar{p} is defined the filtered pressure, Pa; the superscript “—” means filtered; ρ is the density, kg/m³; τ_{ij} is the sub-grid stress and is shown in formula Equation (6):

$$\tau_{ij} = \overline{u_i u_j} - \bar{u}_i \bar{u}_j \quad (6)$$

In the sub-grid model, τ_{ij} is the sub-grid stress tensor, as shown below:

$$\tau_{ij} = (\overline{u_i u_j} - \bar{u}_i \bar{u}_j) = \frac{1}{3} \tau_{kk} \delta_{ij} - 2\mu_{sgs} \left(\overline{S_{ij}} - \frac{1}{3} \overline{S_{kk}} \delta_{ij} \right) \quad (7)$$

where $\overline{S_{ij}} = \frac{1}{2} \left(\frac{\partial \bar{u}_i}{\partial x_j} + \frac{\partial \bar{u}_j}{\partial x_i} \right)$ is the strain rate tensor, $\mu_{sgs} = \bar{\rho} (C_S \Delta)^2 |\overline{S}|$ is called eddy viscosity in the Smagorinsky model, Δ is the filter width and $|\overline{S}| = \sqrt{2 \overline{S_{ij}} \overline{S_{ij}}}$ is the strain rate, and C_S indicates the Smagorinsky coefficient.

2.3. Surface Tension Model

The continuous surface force model (CSF) and the continuous surface stress model (CSS) are applied to modeling for surface tension in Fluent. The CSF is calculated in Equation (8) [30]:

$$\vec{F}_S = \sigma \lambda(l) \delta(\vec{r}) \vec{n} \quad (8)$$

where σ is the surface tension coefficient; $\delta(\vec{r})$ is the Dirac delta function; $\lambda(l)$ is the curvature at the position of l ; \vec{n} is the unit normal vector at the interface.

$$\vec{n} = \nabla c(a) \quad (9)$$

where $c(a)$ is the color scale function. $\lambda(l)$ is calculated as:

$$\lambda(l) = -(\nabla \cdot \vec{n}) \quad (10)$$

3. Numerical Model

3.1. Geometrical Model

The actual size of Lanzhou–Jiangyou section of Lan–Cheng–Yu pipeline is taken as the model size, and a pipeline with a diameter of 508 mm is adopted. As shown in Figure 1, the actual wall thickness is δ , the length of the horizontal pipe section is L_1 , the inclined pipe section is L_2 , the angle between the horizontal pipe and inclined pipe is α , and the radius of curvature is R . The specific parameters of the model are listed in Table 1. The left side of the horizontal section is an oil phase inlet, and the right side of the inclined section is the oil-water outlet.

Table 1. Parameters of the geometrical model.

L_1 (m)	L_2 (m)	D (mm)	δ	R (mm)
10	10	508	9	2450

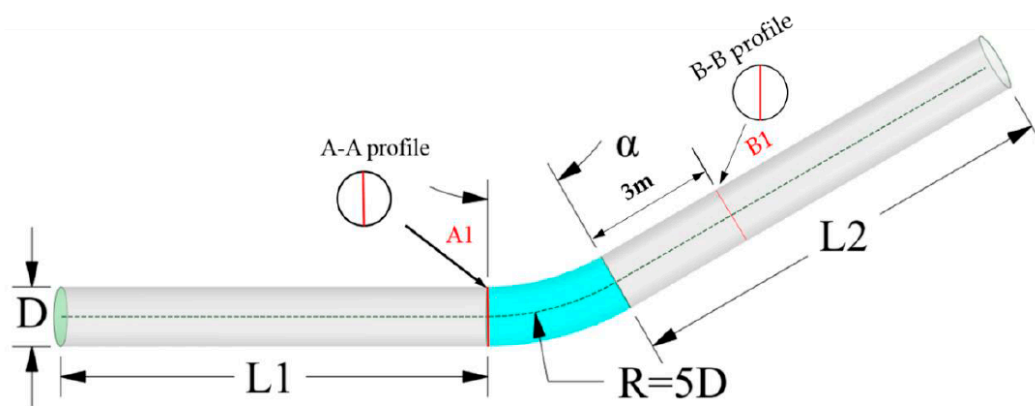


Figure 1. Geometrical model of the pipeline.

3.2. Mesh Generation

In order to ensure the calculation accuracy, the model in Figure 1 is divided into a block-structured mesh. The mesh division and mesh quality inspection results are listed in Figures 2 and 3, respectively.

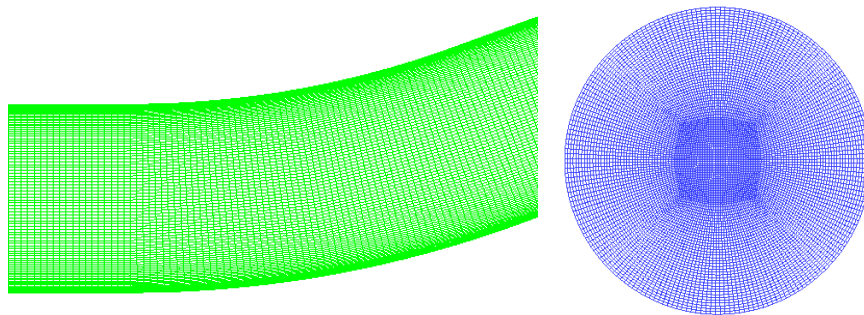
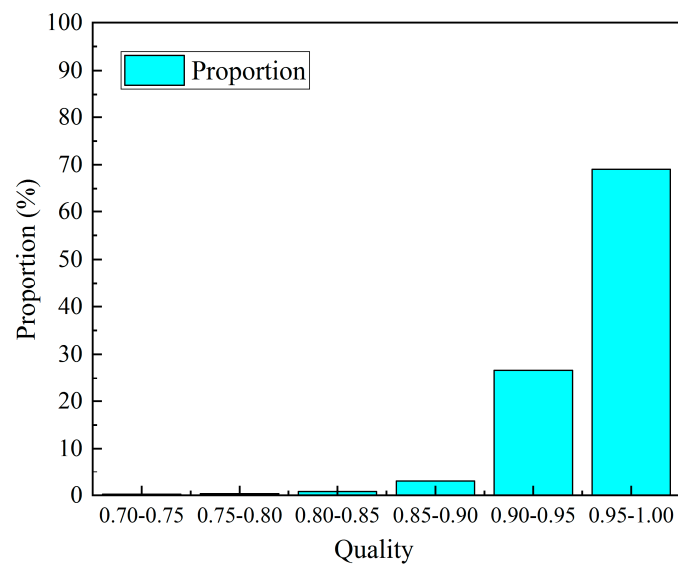


Figure 2. Mesh generation.



(a) Quality

Figure 3. Cont.

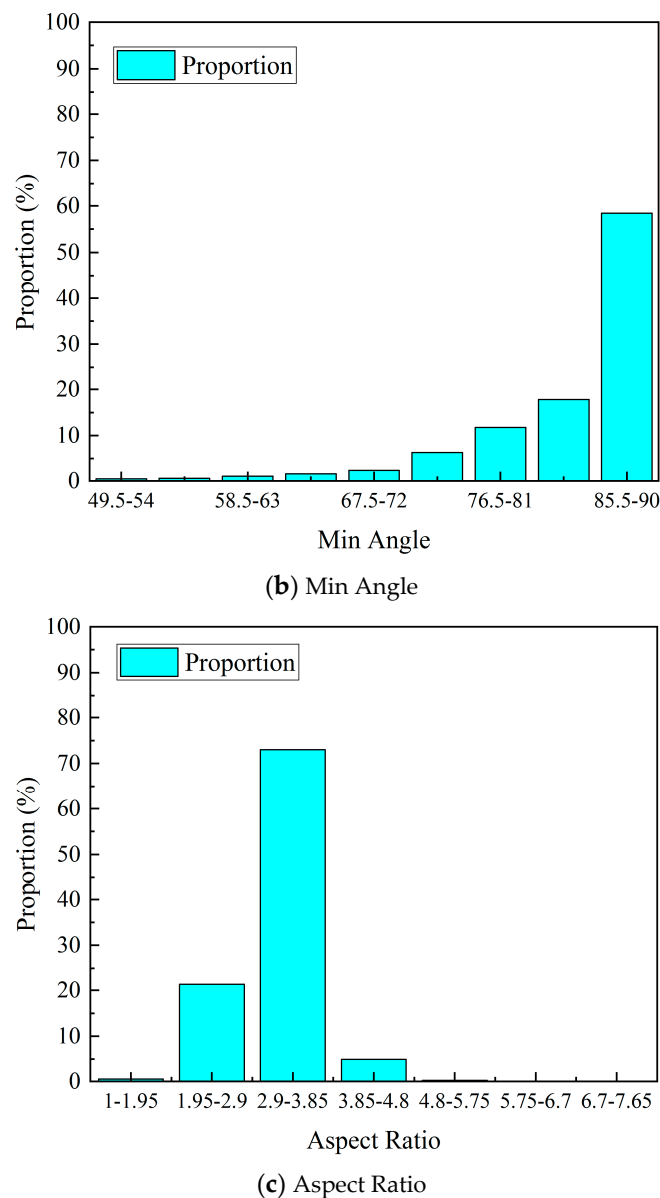


Figure 3. Results of mesh quality inspection.

3.3. Parameter Settings

The oil phase inlet is set to the velocity inlet. Since the annual oil transportation volume of Lanzhou–Jiangyou section in recent years is between $304\sim 608 \times 10^4$ t [10], the speeds are 0.66, 0.88, 1.11, 1.33, and 1.55 m/s, with an interval of 0.22 m/s. All velocities at the inlet section of the pipe are the same. The turbulent intensity at the inlet of the pipe is 5% considering the inlet pulsation. The oil-water outlet is set as an outflow. The part around the pipe adopts the no-slip wall boundary. The initial water content is set as shown in Figure 4 and h is 150 mm. The length of the assumed water region is 5 m along the pipe length. At the beginning of the simulation, the initial velocities of the water phase and the oil phase in the pipeline are assumed to be 0 m/s. This is an ideal hypothesis. However, since both fluids are incompressible, the state in the pipe is consistent with the actual flow when the flow begins. In addition, the pipeline in the Lanzhou–Jiang oil section is highly undulating, with inclined angles ranging from 10° to 40° , so four sets of inclined angles of 10° , 20° , 30° , and 40° are selected. The physical properties of diesel oil and water at 20°C are listed in Table 2.

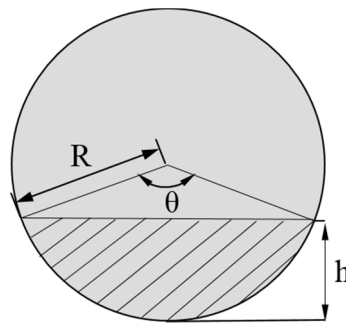


Figure 4. Initial water content.

Table 2. Physical parameters.

Medium	Dynamic Viscosity/mPa·s	Density/kg·m ⁻³
Diesel oil	3.575	908.2
Water	1.03	1000
Surface tension	0.01795 N/m	

3.4. Numerical Methods

Numerical methods play an important role in simulation research and different methods often get different simulation results. LES method was used for numerical simulation and the specific model and solution method was shown in Table 3.

Table 3. Model and numerical solution methods.

Specification	Category	Methods
Turbulence model	LES	Smagorinsky–Lilly
Pressure-velocity coupling	Scheme	PISO
Spatial discretization	Gradient	Least square cell based
	Pressure	PRESTO!
	Momentum	Bounded central differencing
	Volume fraction	First order upwind

3.5. Mesh Independence Verification

Under the same operating conditions, five grids with the model inclination of 30° and the number of meshes of 1,754,910, 2,889,432, 3,849,120, 4,368,125, and 5,706,880 were simulated to verify the mesh independence. The time step size is 0.005 s. The velocity distribution at B1 of the B-B profile in Figure 1 was extracted for comparative analysis to determine the appropriate mesh model.

The inlet velocity of the oil was set at 1.11 m/s, and other settings were consistent. The above five meshes were used to simulate the process. As the flow time is 8 s, the velocity magnitude curve at B1 is shown in Figure 5. This velocity is the instantaneous velocity magnitude at B1 in Figure 1. As shown in the figure, when the number of meshes gradually increases, the change in velocity decreases. As the mesh numbers are 4,368,125 and 5,706,880, the velocities are basically the same. To improve the efficiency and accuracy of calculation, the mesh model with 4,368,125 is taken as the final calculation model.

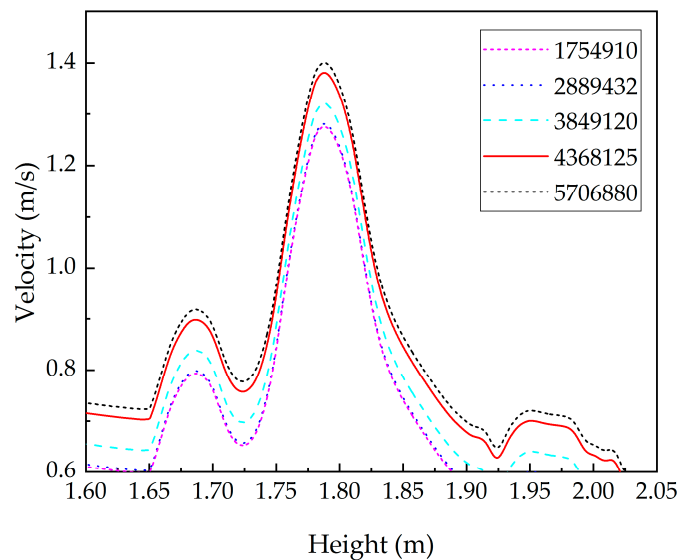


Figure 5. Mesh independence verification.

3.6. Analysis of y^+

The results have shown that the calculation results of y^+ between 0 and 30 in the LES method are the most accurate [32,33]. Therefore, the distribution of the y^+ value in the pipeline direction when the flow time is 15 s is extracted in Figure 6. The value of y^+ along the pipeline is between 2 and 50, which meets the requirements of calculation accuracy required for LES.

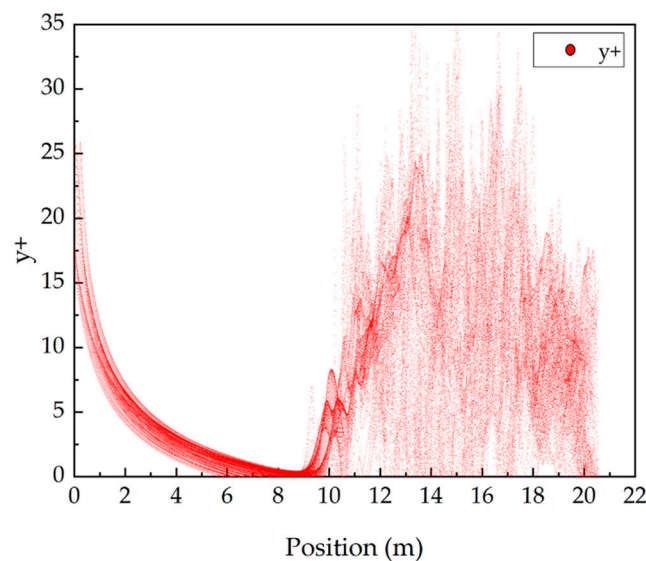


Figure 6. y^+ along the pipeline.

4. Analysis of Simulation Results

4.1. Method Verification

An inclined pipe model was established by Tao Zhang et al. [29] to verify the application of the LES method with diameter $D = 50$ mm, horizontal part $L_1 = 1000$ mm, inclined part $L_2 = 1000$ mm, and curvature radius $R = 5D = 250$ mm. Under the conditions of corresponding parameters, the LES simulations are compared with the experimental data by means of experimental observation and simulation verification. The results show that the experimental and simulation results of the oil carrying water process are highly consistent, which proves that LES can be applied to the simulation

of carrying water. Figure 7 shows the oil-water distribution of experimental results and simulation results with $v = 0.25$ m/s, $\alpha = 10^\circ$ and 40° .

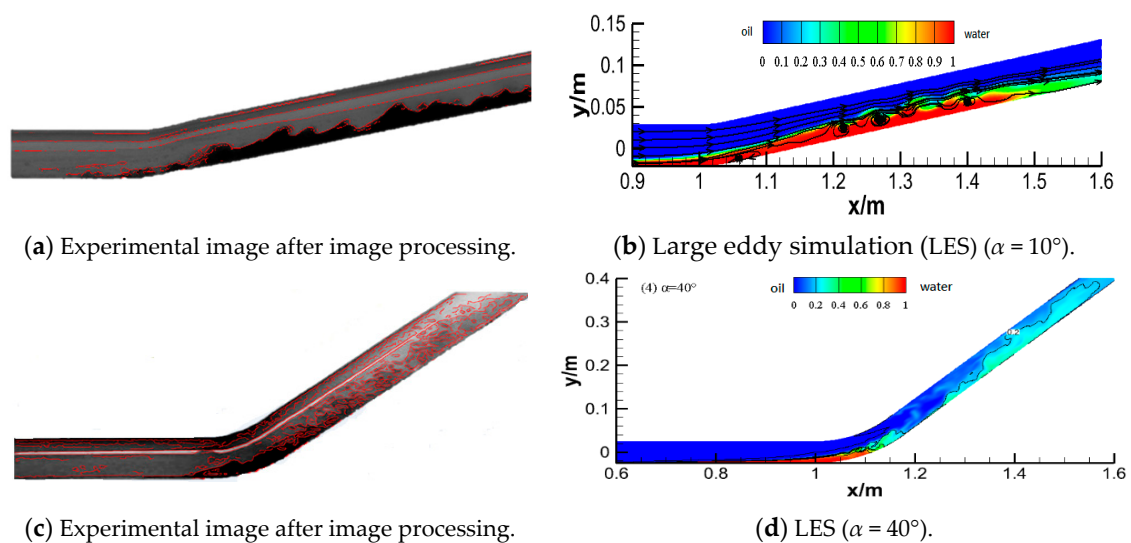


Figure 7. Comparison of two methods ($t = 3$ s) [29].

The flow pattern presents a wavy stratified flow in Figure 7a. The water in the horizontal section gradually enters the inclined section, and most of the water is mainly concentrated in the lower part of the inclined pipe, and obvious wavy stratification appears at the oil-water interface. In Figure 7b, the contour of the LES method shows a wavy stratified flow, the oil-water interface is evenly distributed and there is a phenomenon of mutual mixing at the interface, which is consistent with the experimental results. In addition, the streamline was distorted and formed a vortex, and then formed a wave structure in the process of oil carrying water. As shown in Figure 7d, there is a smooth stratified flow pattern in the horizontal section. As the water is carried to the inclined part of the pipeline by oil, the water is quickly dispersed into the oil to form a dispersed flow pattern, which basically conforms to the Figure 7c flow pattern characteristics.

The comparative analysis of the experimental and simulation results under the two operating conditions proves that the LES method can identify the flow characteristics of oil carrying water. It is in good agreement with the experimental results, which can be used for the study of the law of oil and water.

4.2. Processes of Oil Carrying Water

The water-carrying process of oil is a typical transient flow process. The LES is used to simulate the dynamic water carrying process of Lan–Cheng–Yu pipeline. As the inclined angle α is 10° and the oil inlet velocity v is 1.33 m/s, the contours of the water-carrying process are shown in Figure 8.

As shown in Figure 8, the flow in the pipe is at the initial stage of 1~8 s, the oil-water interface is smooth, and there is no mixing phenomenon. The water flows to the inclined section in a smooth stratified flow pattern with the displacement function of the oil. As the time is between 9~14 s, the water is carried by the oil phase into the inclined section. The kinetic energy of water is gradually transformed into potential energy, velocity decreases, oil-water velocity difference increases, shear effect increases, and the stratified flow transforms into a wave-like stratified flow. As flow time is 15~19 s, the oil-water is mixed, the oil flow area decreases and the velocity increases at the crest, while the oil flow area increases and the velocity decreases at the trough. The fluctuation between crest and trough gradually develops into a vortex, resulting in more severe disturbance of the oil-water interface. Then the flow pattern appears as a dispersed flow.

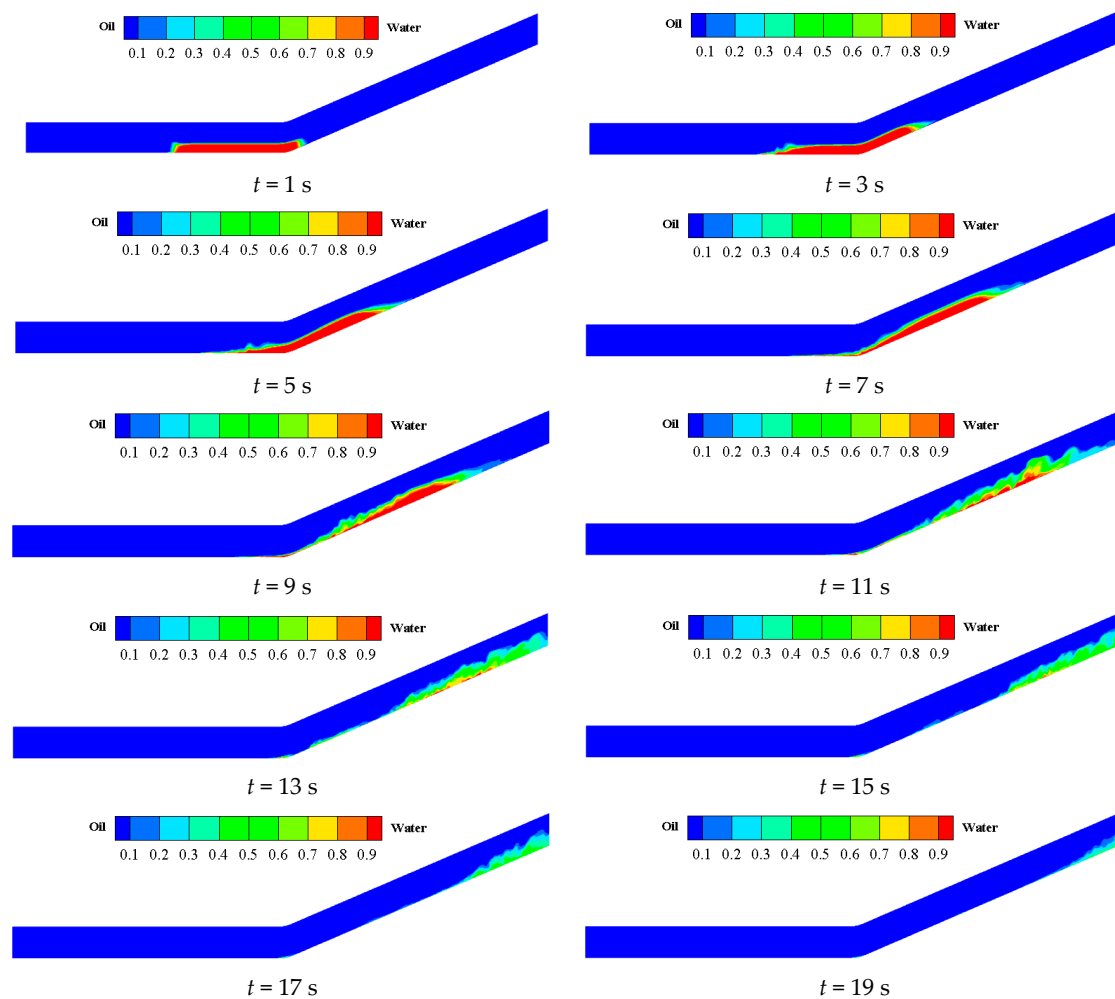


Figure 8. Phase distribution of water-carrying process ($\alpha = 10^\circ$).

Figure 9 is the contours of the water-carrying process of the oil as the inclined angle α is 30° and the inlet velocity is 1.33 m/s. As the flow time is 1~8 s, the oil phase has just entered the pipeline. The inclined section presents a smooth stratified flow, and the oil-water interface is evenly distributed with little disturbance. As the flow time is 9 s, the flow time increases, the oil-water velocity difference increases, the front end of the water and the oil phase are mixed with each other, and the water content decreases. At this time, the stratified flow becomes a wavy stratified flow. As flow time is 10~19 s, the flow state is turbulent, the fluid in the pipe pulsates violently, the oil-water mixing in the inclined pipe is serious, the shearing action is great, and the flow pattern develops into a dispersed flow.

The Lan-Cheng-Yu product oil pipeline fluctuates greatly in Figures 8 and 9. The flow patterns in the pipeline are mainly stratified flow, wavy stratified flow, and dispersed flow. In addition, the transition time of flow patterns is different under various operating conditions.

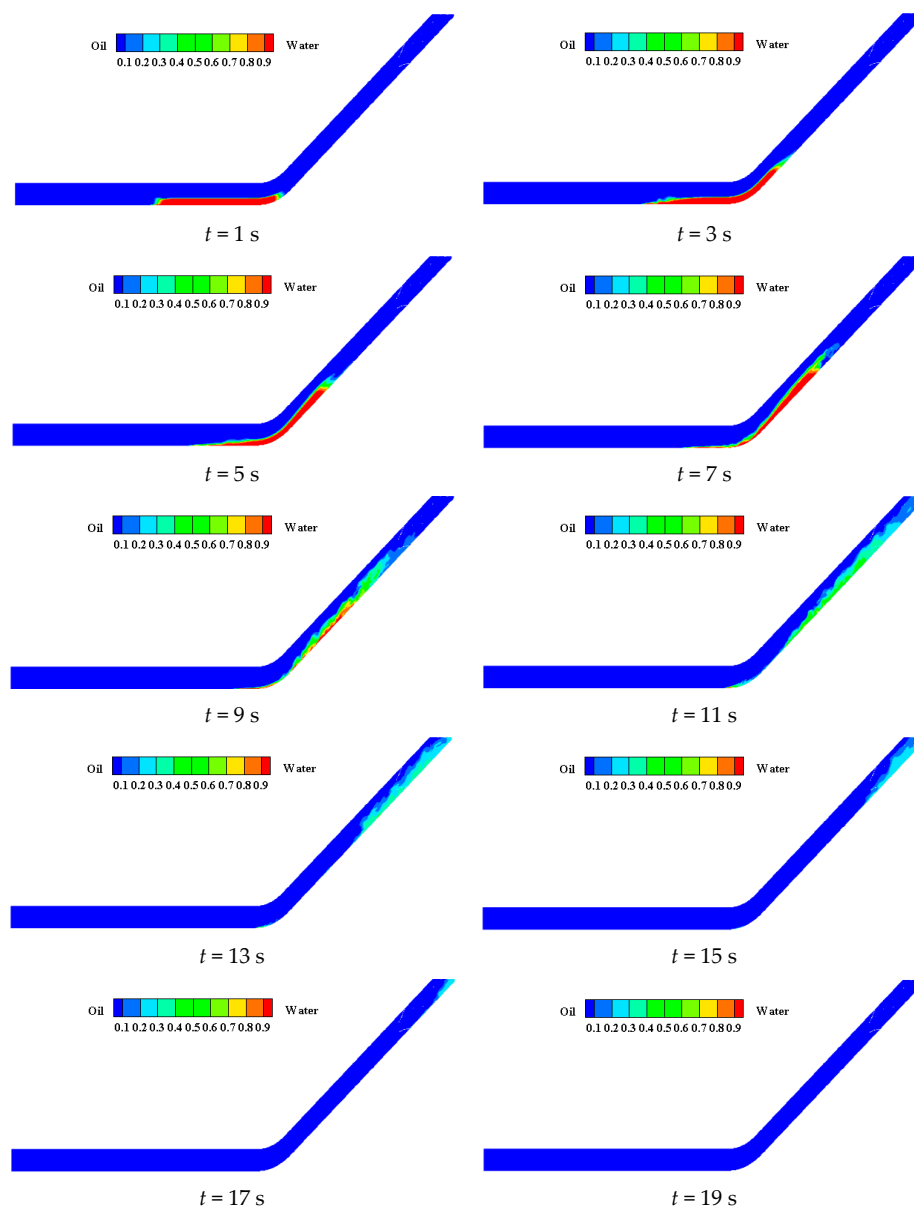


Figure 9. Phase distribution of water-carrying process ($\alpha = 30^\circ$).

4.3. The Transition of Flow Patterns

4.3.1. Distribution of Two Phases

The variation laws of flow pattern in the process of oil carrying water in Lan–Cheng–Yu pipeline under variable oil inlet velocities and angles were studied with the above-mentioned numerical model.

Figure 10 shows the oil-water distribution and streamline diagram under different oil phase inlet flow rates as the flow time is $t = 11$ s and the pipeline inclined angle is $\alpha = 10^\circ$. In Figure 10, as the velocity is 0.66~1.11 m/s, the water gradually flows from the bottom of the horizontal section to the inclined section. At this time, the oil-water velocity difference is small, the shear effect is small, the oil-water two-phase interface fluctuates little, and the streamline is less affected by the fluctuation, showing a smooth stratified flow pattern. As the velocity is 1.33~1.55 m/s, the oil-water velocity difference increases, the shearing effect is greater, the oil-water two-phase interface begins to fluctuate, and the oil-water intermixes with each other. The streamlines of the oil-water interface are slightly distorted. The oil and water present a wavy stratified flow and moves to the bottom of the inclined pipe.

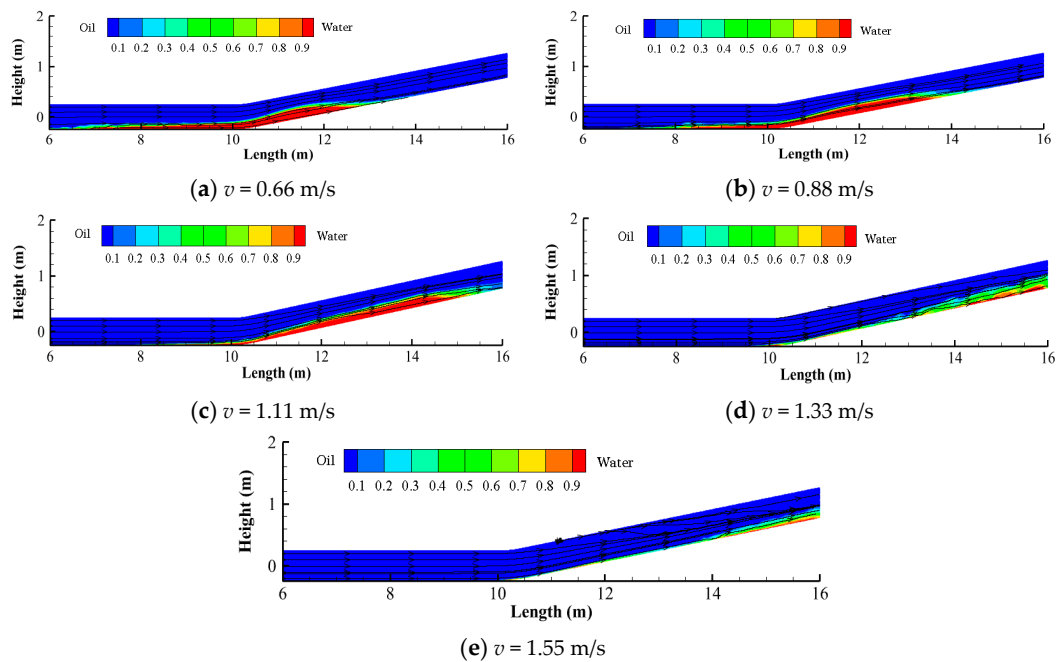


Figure 10. Distribution of oil and water ($\alpha = 10^\circ$, $t = 11.0$ s).

Figure 11 shows the oil-water distribution and streamline diagram at different oil-phase inlet velocities as t is 11 s and α is 20° . As the velocity is 0.66~0.88 m/s, the water phase has not completely entered the bottom of the inclined section, the flow pattern in the horizontal part is stratified flow, and the flow pattern at the bottom of the inclined section has a tendency to transition to wavy stratified flow. As the velocity is 1.11 m/s, the flow of oil and water presents a wavy stratified flow. As the velocity is 1.33~1.55 m/s, the oil-water two phases are mixed with each other, the wavy stratified flow disappears, and the flow flows to the inclined pipe in the form of dispersed flow.

Figure 12 shows the oil-water two-phase distribution and streamline diagram at different oil-phase inlet flow velocities as the flow time t is 11 s and the pipe inclination α is 30° . As the velocity is 0.66~0.88 m/s, the tube presents a smooth stratified flow pattern. The streamline is relatively stable at the oil-water interface. It is seriously distorted at the water phase, forming vortices at the bottom and top of the inclined tube. As the velocity is 1.11 m/s, the stratified flow gradually changes into a wavy stratified flow, and a vortex is performed at the bottom of the inclined tube. When the velocity continues to increase, the vortex disappears and the flow pattern eventually develops into a dispersed flow.

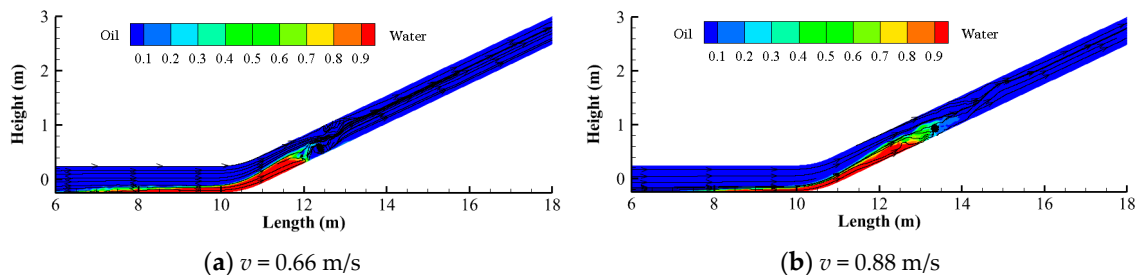


Figure 11. Cont.

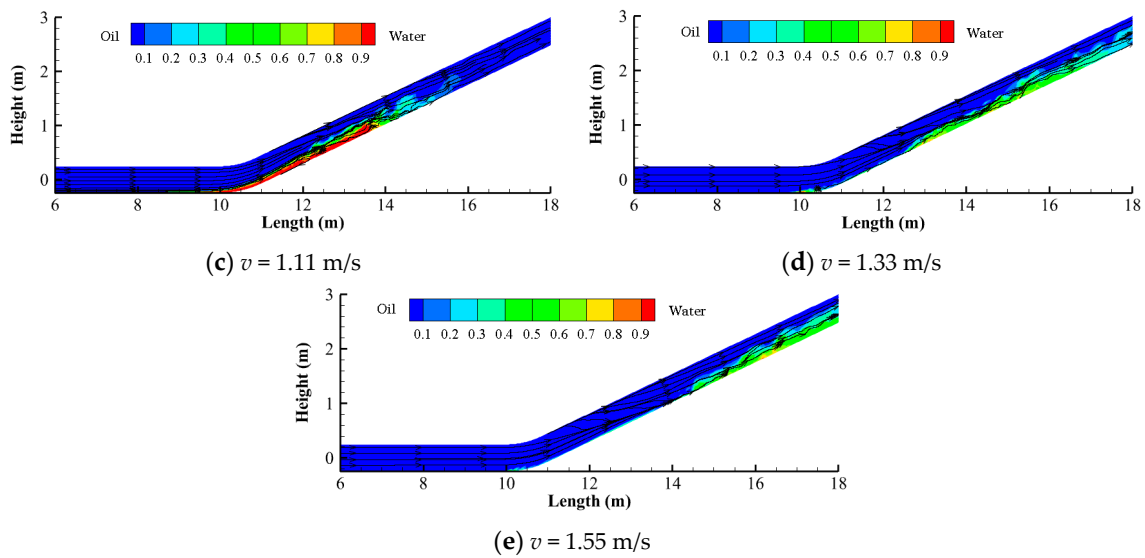


Figure 11. Distribution of oil and water ($\alpha = 20^\circ, t = 11.0$ s).

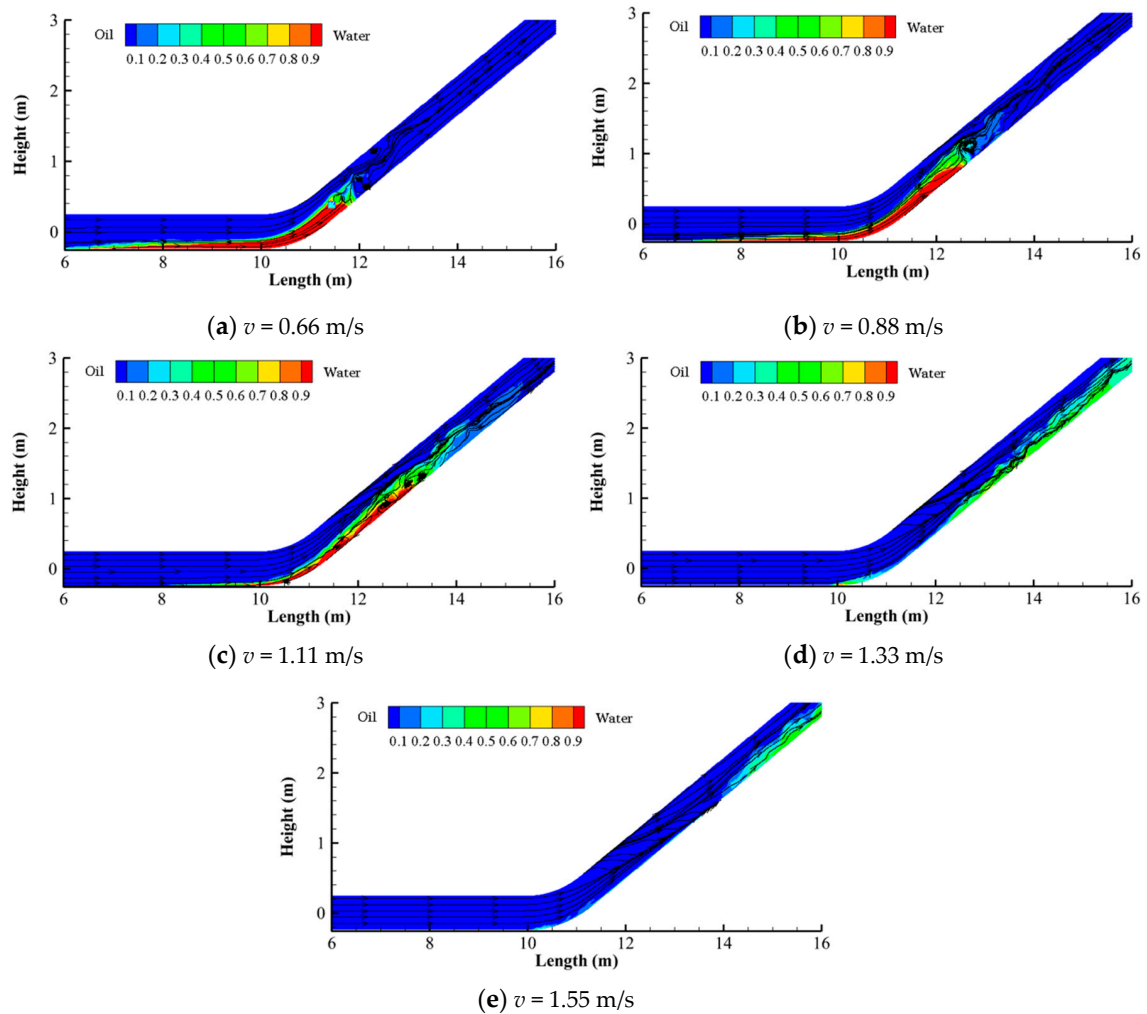


Figure 12. Distribution of oil and water ($\alpha = 30^\circ, t = 11.0$ s).

Figure 13 shows the oil-water distribution and streamline diagram at different oil-phase inlet velocity as the flow time t is 11 s and the pipe inclination α is 40° . As the velocity is 0.66 m/s, the oil-water

interface is evenly distributed and the flow pattern is stratified flow. The streamline behind the water phase is greatly affected by disturbance, and vortices exist in every position of the inclined pipe. As the oil inlet velocity is 0.88 m/s, the streamline distortion range increases, the vortex is mainly concentrated on the bottom of the inclined tube, and the flow is wavy stratified flow. As the velocity is 1.11 m/s, the flow pattern is dispersed flow. There is a vortex at the bottom of the inclined pipeline. When the velocity continues to increase, the vortex disappears, the oil carries the water and flows out from the right side of the inclined pipe in a dispersed flow pattern.

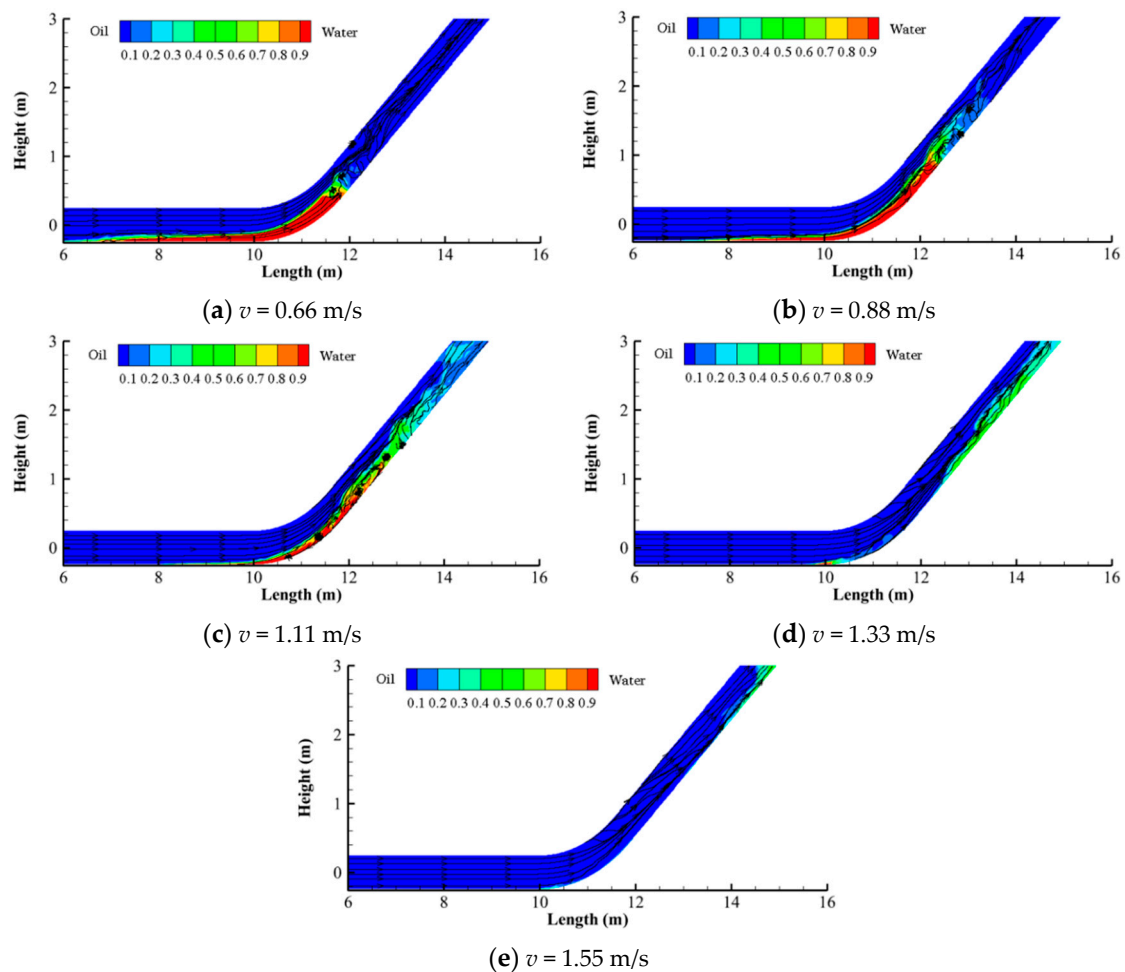


Figure 13. Distribution of oil and water ($\alpha = 40^\circ$, $t = 11.0$ s).

According to the four inclined angles, the flow patterns in the inclined part change with flow time as the inlet velocity is 0.66~1.55 m/s, shown in Figure 14. There are three main flow patterns in the pipe, such as stratified flow, wavy stratified flow, and dispersed flow. As the pipe inclined angle is fixed and the oil inlet velocity is low, the two phases enter into the inclined pipe at a certain velocity difference due to the carrying effect of oil to the water phase. At this time, the flow pattern is smooth and stratified flow. After a period of time, the kinetic energy of the mixed fluid is gradually transformed into potential energy in the inclined part. The velocity difference between the two phases is further increased on account of the difference of oil-water content and density, which leads to the increase of shear action, the increasingly severe fluctuation of the interface, and the change of flow pattern from stratified flow to wavy stratified flow. When the inlet velocity of the oil phase continues to increase, the shear action is enhanced, the flow state in the pipe is turbulent, the pulsation is very severe, the mixing degree of oil and water is deepened, and the flow pattern tends to a dispersed

flow. In addition, the transition time of flow patterns is gradually advanced with the increase of oil inlet velocity.

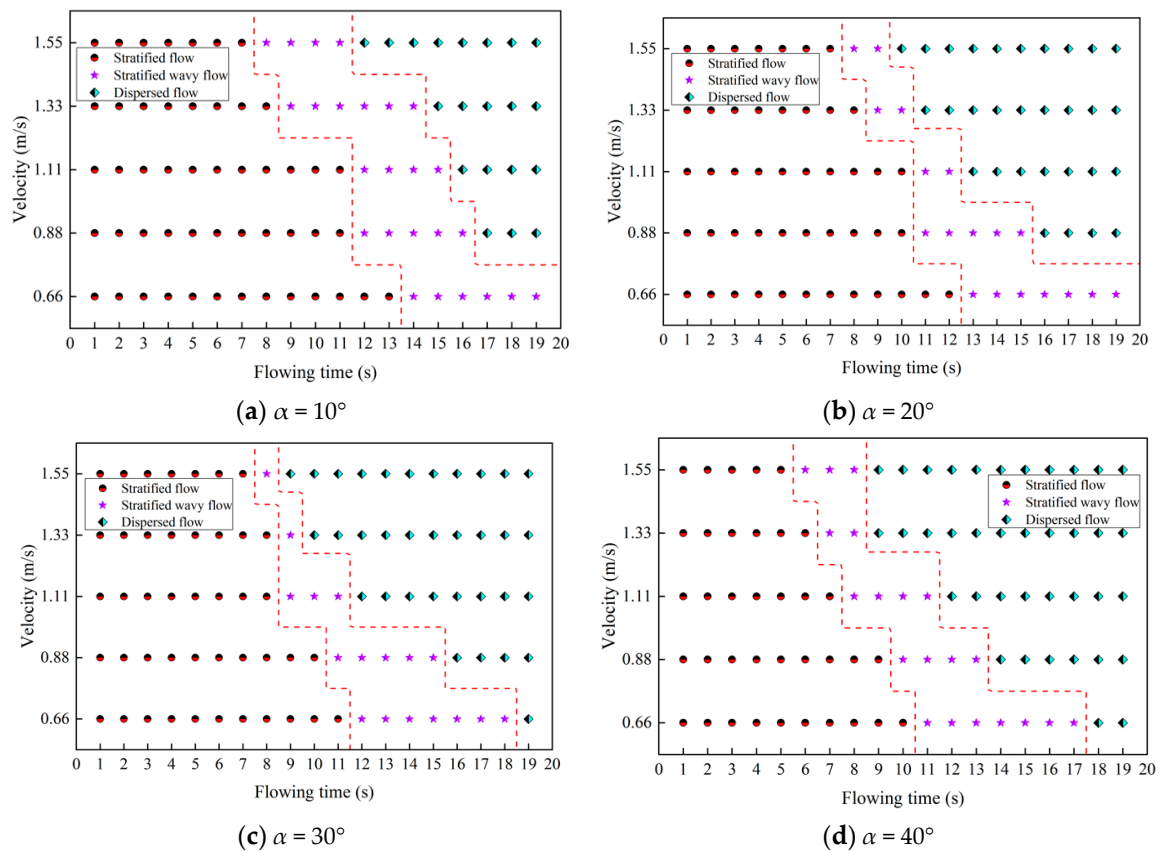


Figure 14. Flow pattern changes under various operating conditions.

As the oil inlet velocity is fixed, the oil flow carries the water phase into the inclined section. With the increase of velocity difference between two phases in the inclined section, the oil-water shearing action increases, and the flow pattern changes from stratified flow to wavy stratified flow. At this time, when the inclined angle of the pipeline gradually increases, the wavy stratified flow becomes a dispersed flow. As the inlet velocity of oil is fixed, the transition time of time for the flow patterns is also accelerated with the increase of pipeline inclination.

4.3.2. Distribution of Oil-Water Velocity

To observe the velocity distribution at different inlet velocities, the velocity distribution in the pipe under the conditions of 20° and 40° inclined angles were studied.

Figure 15 performs the velocity distribution in the pipe at different oil phase inlet flow velocities when the flow time is 11 s and the pipe inclination is 20° . As shown in the figure, the places with higher speed in the pipe are mainly concentrated at the upper part of the inclined pipe, and the velocity at the bottom of the inclined tube is relatively slow. And the area with higher velocity gradually moves to the outlet position of the pipeline with the increase of the oil inlet velocity.

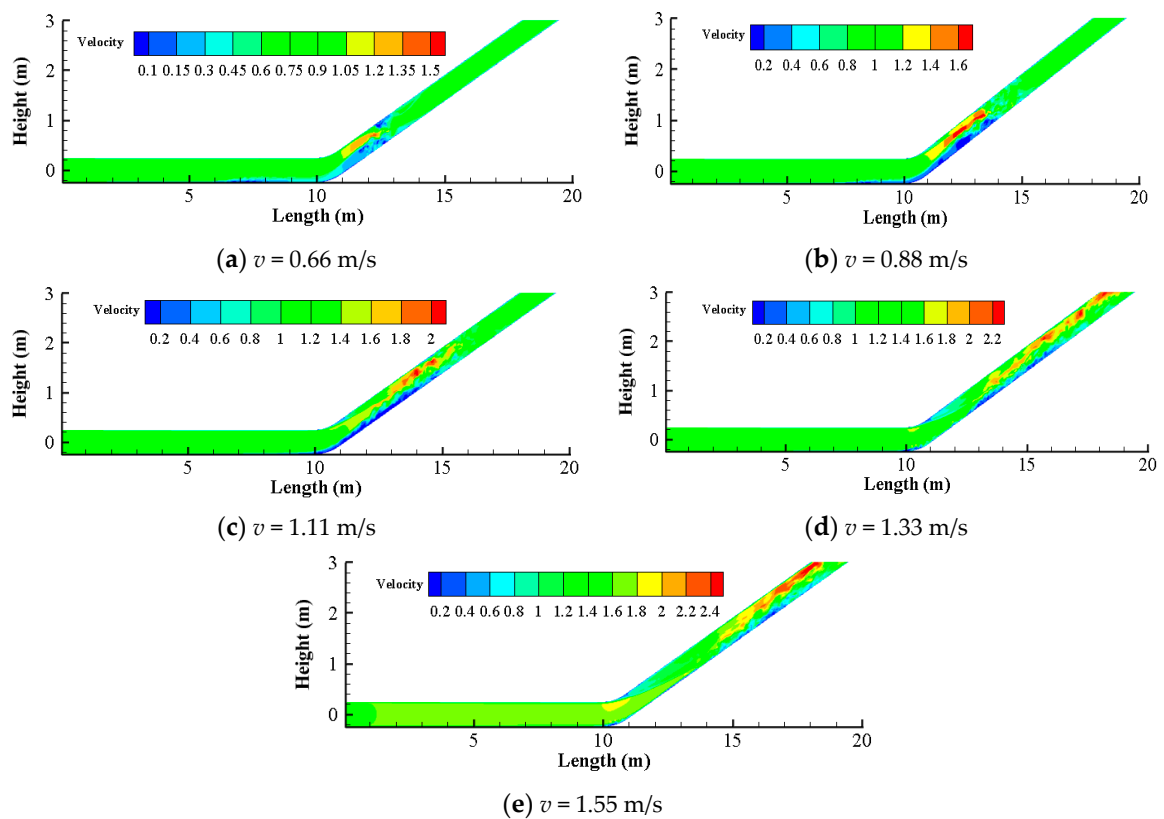


Figure 15. Velocity distribution in pipe at $\alpha = 20^\circ$ ($t = 11.0$ s).

As the inclined angle α is 20° and the flow time is 11.0 s, the velocity distribution, and shear rate distribution at A1 on section A-A in Figure 1 are shown in Figure 16. As shown in Figure 16a, velocities at the bottom and upper section are relatively small, while the velocity in the middle part is relatively large and evenly distributed. With the increase of oil inlet velocity, the velocity in the middle of the pipeline also increases gradually. Among them, the inlet oil phase velocities are 0.66 m/s, 0.88 m/s, 1.11 m/s, 1.33 m/s, and 1.55 m/s, and the corresponding maximum velocities are 0.79 m/s, 1.06 m/s, 1.30 m/s, 1.58 m/s, and 1.82 m/s, respectively.

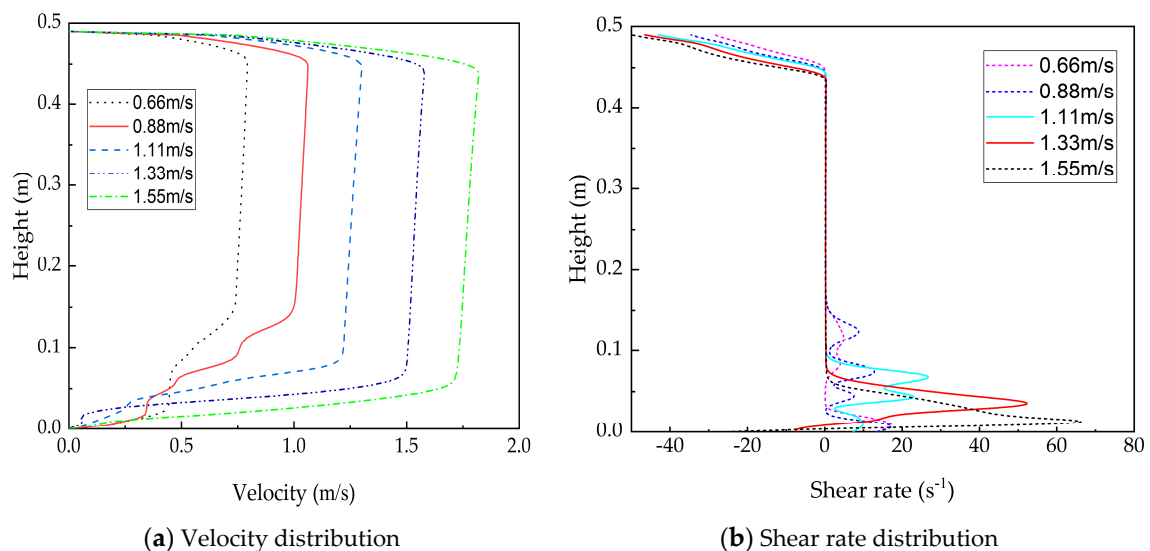


Figure 16. Velocity distribution and shear rate distribution of the A-A section ($\alpha = 20^\circ$).

In Figure 16b, the maximum shear rate 17.5 s^{-1} corresponding to 0.66 m/s appears at $y = 9 \text{ mm}$; the maximum shear rate 18.2 s^{-1} corresponding to 0.88 m/s appears at $y = 7 \text{ mm}$; the maximum shear rate 28.0 s^{-1} corresponding to 1.11 m/s appears at $y = 68 \text{ mm}$; the maximum shear rate of 54.1 s^{-1} corresponding to 1.33 m/s appears at $y = 36 \text{ mm}$; and the maximum shear rate of 67.5 s^{-1} corresponding to 1.55 m/s appears at $y = 14 \text{ mm}$. In conclusion, as the oil inlet velocity was 0.66 m/s and 0.88 m/s , the oil-water velocity difference was small and the maximum shear rate was small. As the oil inlet velocity is $1.11\text{--}1.33 \text{ m/s}$, the velocity increases, so does the oil-water velocity difference and the shear rate. The region with the maximum positive shear rate gradually moves from the lower part of the pipeline to the bottom of the pipeline with the increase of the velocity.

Figure 17 is a contour of the velocity distribution in the pipe under different oil phase inlet flow rates when the flow time is 11 s and the pipe inclination α is 40° . As shown in the figure, when the velocity is 0.66 m/s , the velocity at the bottom and top of the inclined section is smaller while largest in the middle. When the velocity is $0.88\text{--}1.11 \text{ m/s}$, the velocity at the top of the pipeline increases with the increase of velocity, and the area with higher velocity flows along the top of the pipeline to the outlet of the pipeline. When the velocity is 1.33 m/s , the velocity distribution in the pipeline is relatively uniform except for the high-speed area. When the velocity continues to increase, the velocity distribution in the pipe is uniform, and the oil flow basically carries the water out of the inclined section.

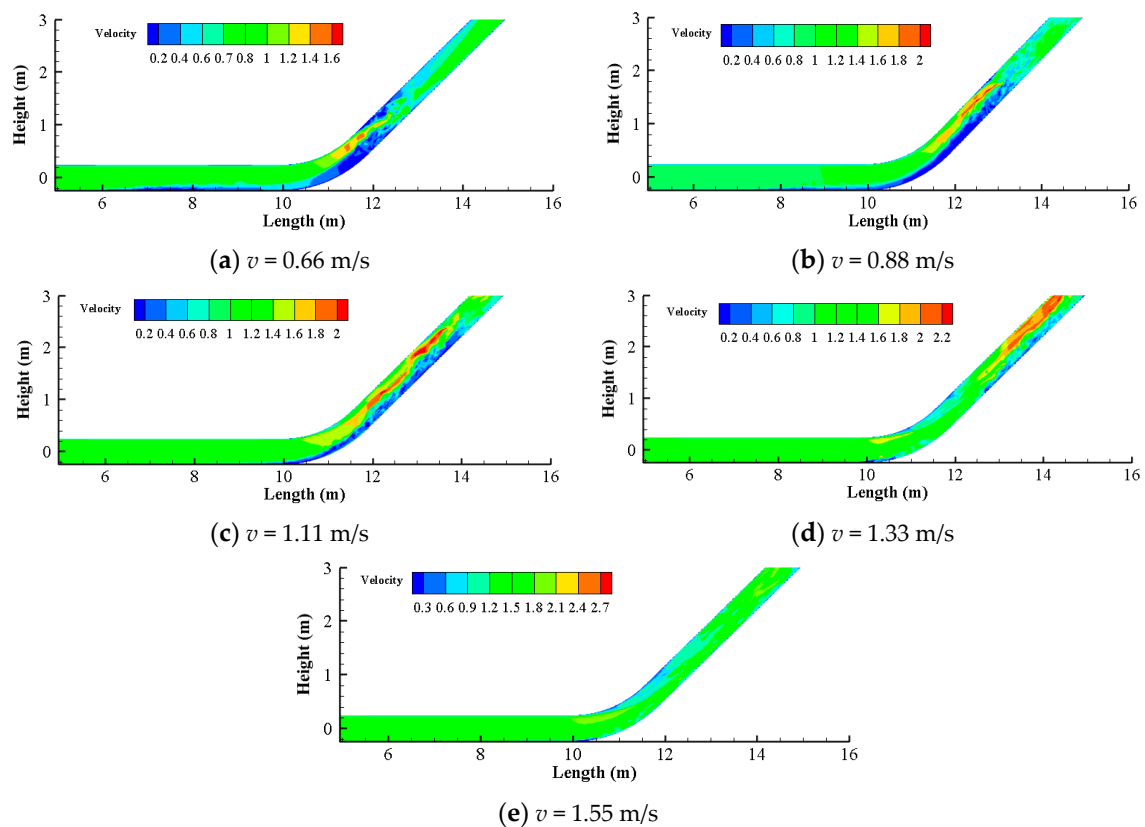


Figure 17. Contour of velocity distribution in pipe at $\alpha = 40^\circ$ ($t = 11.0 \text{ s}$).

The velocity distribution and shear rate distribution at section A1 of A-A in Figure 1 are shown in Figure 18 at $\alpha = 40^\circ$ and $t = 11.0 \text{ s}$. As the inclined angle α is 40° , the velocity distribution at section A1 of A-A is basically consistent with that when α is 20° . The maximum velocities at 0.66 m/s , 0.88 m/s , 1.11 m/s , 1.33 m/s , and 1.55 m/s are 0.80 m/s , 1.07 m/s , 1.30 m/s , 1.58 m/s , and 1.82 m/s , respectively. It can be seen that the change of the pipeline inclination has little effect on the velocity distribution and the maximum velocity of the inclined pipe section entrance section.

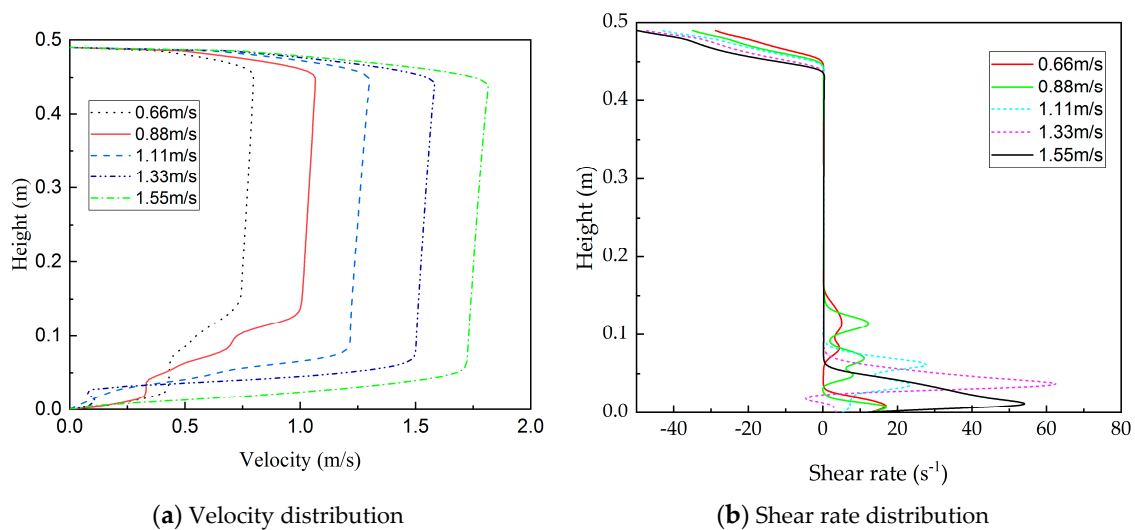


Figure 18. Velocity distribution and shear rate distribution in section A-A ($\alpha = 40^\circ$).

As shown in Figure 18b, when the flow time is 11.0 s and the inclined angle α is 40° , the maximum shear rate of 18.6 s^{-1} corresponding to 0.66 m/s appears at $y = 9 \text{ mm}$; the maximum shear rate of 18.9 s^{-1} corresponding to 0.88 m/s appears at $y = 7 \text{ mm}$; the maximum shear rate of 28.1 s^{-1} corresponding to 1.11 m/s appears at $y = 59 \text{ mm}$; the maximum shear rate of 1.33 m/s corresponding to 63.0 s^{-1} appears at $y = 36 \text{ mm}$; the maximum shear rate of 54.8 s^{-1} corresponding to 1.55 m/s appears at $y = 9 \text{ mm}$. In conclusion, when the oil inlet velocity is 0.66~0.88 m/s, the oil-water velocity difference is small and the maximum shear rate is small. At this time, the oil flow just begins to carry the water phase, and the shear rate near the pipe wall is the highest; When the oil inlet velocity increases from 1.11 m/s to 1.33 m/s, the oil inlet velocity increases, the oil-water interface fluctuates sharply, the water phase decreases gradually, the oil-water interface moves down, and the maximum positive shear rate also increases and moves down. As the oil velocity is 1.55 m/s, the water in the pipeline basically disappeared. The velocity of water increases after being carried by oil. At this time, the oil-water velocity difference decreases, and the maximum positive shear rate decreases.

4.4. Analysis of Water Carrying Capacity

The process of oil carrying water can determine the changing characteristics of oil-water flow patterns under the influence of different oil inlet velocity and pipeline inclined angle. In addition, the variation law of water accumulation with time is more important to the engineering practice when the oil inlet velocity and pipe inclined angle are different.

Figure 19 shows the variation curve of water accumulation mass with flow time under different velocities at $\alpha = 10^\circ, 20^\circ, 30^\circ$, and 40° . The mass of the water in the pipe gradually decreases with the increase of the flow time. In addition, the mass of the water in the pipe decreases with the increase of the oil inlet velocity. As the inclined angle of the pipeline is 10° , the oil inlet velocity is 0.66 m/s, 0.88 m/s, 1.11 m/s, 1.33 m/s, and 1.55 m/s, the corresponding time for the water to be completely output from the pipe is 90 s, 55 s, 36 s, 35 s, and 25 s, respectively. As the inclined angle of the pipeline is 20° , the oil inlet velocity is 0.66 m/s, 0.88 m/s, 1.11 m/s, 1.33 m/s, and 1.55 m/s, the corresponding time for the water to be completely output from the pipe is 85 s, 48 s, 33 s, 23 s, 22 s, respectively. As the inclined angle of the pipeline is 30° , as the oil inlet velocity is 0.66 m/s, 0.88 m/s, 1.11 m/s, 1.33 m/s, 1.55 m/s, the corresponding time for the water to be completely output from the pipe is 92 s, 49 s, 37 s, 24 s, 23 s, respectively. As the inclined angle of the pipeline is 40° , as the oil inlet velocity is 0.66 m/s, 0.88 m/s, 1.11 m/s, 1.33 m/s, 1.55 m/s, the corresponding time for the water to be completely output from the pipe is 95 s, 50 s, 39 s, 26 s, 25 s, respectively.

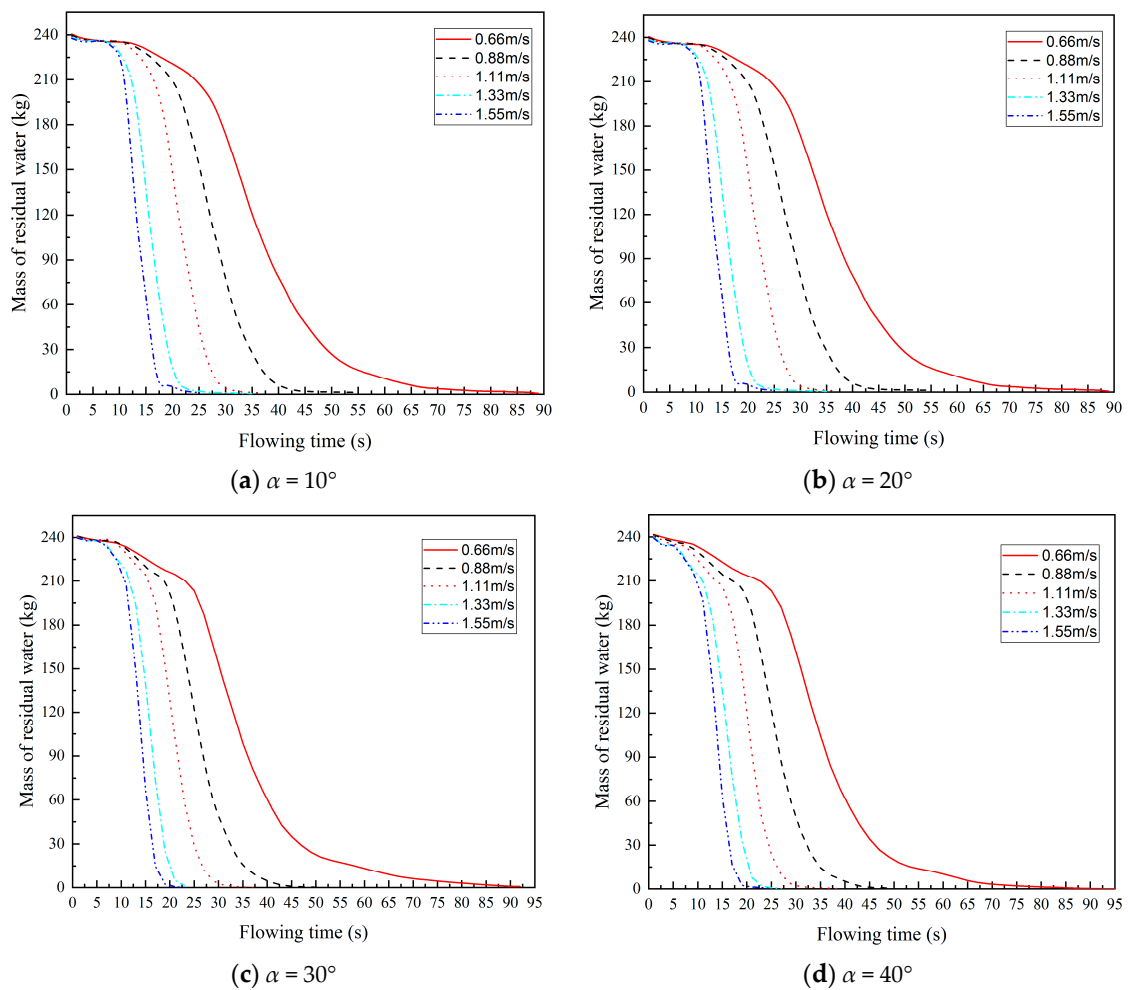


Figure 19. The remaining mass change curve of the water in the pipe.

To sum up, when the inclined angle of the pipeline is the same, the water carrying capacity of oil flow increases with the increase of oil inlet velocity. In addition, when the inclined angle of the pipeline changes, the time required to completely carry the accumulated water in the pipeline out of the pipeline under different inclined angles are shown in Figure 20. As the inclined angle increases from 10° to 20° , the power of part of the water mass moving along the inclined pipe is mainly caused by the shearing action of the high-speed oil and water. At this time, the water-carrying capacity of the oil is gradually increased. The time to completely carry water out of the pipeline is shortened. As the inclined angle of the pipeline increases from 20° to 40° , the increase in the inclined angle of the pipeline gradually converts the kinetic energy of the oil phase into gravitational potential energy, resulting in insufficient water-carrying power of the oil phase and reduced water-carrying capacity, and the oil phase will completely carry out the water. The time required for the pipeline gradually increases. Therefore, as the inclination of the pipeline increases, the water-carrying capacity of oil first increases and then decreases.

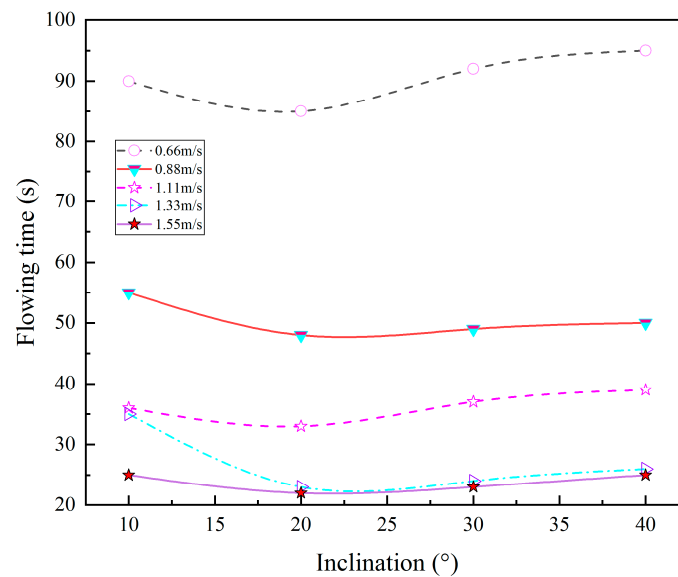


Figure 20. The time required for carrying water by oil with different inclined angles.

5. Conclusions

(1) A numerical model based on LES-VOF in the small-diameter pipeline was established. It was applied to study the law of oil carrying water in Lanzhou–Jiangyou section of Lan–Cheng–Yu product oil pipeline. Combined with the research literature on the small pipe diameter and the simulation results of Lan–Cheng–Yu pipeline, it can be seen that the flow patterns in the pipeline of oil carrying water in both large pipe diameter and small pipe diameter mainly include stratified flows, wavy stratified flows, and dispersed flows.

(2) As the pipeline inclined angle is 10~20° and the oil inlet velocity is 0.66 m/s, the flow patterns in the pipeline mainly include stratified flows and wavy stratified flows. As the oil inlet velocity is 0.88~1.55 m/s, the flow patterns in the pipe are mainly stratified flow, wavy stratified flow, and dispersed flow. As the inclined angle of the pipeline is 30~40°, there are three main types of flow in the pipeline: stratified flows, wavy stratified flows, and dispersed flows. The increase of oil inlet velocity accelerates the transition between different flow patterns.

(3) As the maximum positive shear rate is less than or equal to 17.5 s^{-1} , the flow pattern in the pipe is a stratified flow. As the maximum positive shear rate is between $18.2\text{--}28.1 \text{ s}^{-1}$, the flow pattern in the pipe is a wavy stratified flow. As the maximum positive shear rate is between $54.1\text{--}67.5 \text{ s}^{-1}$, the flow pattern in the pipe is a dispersed flow.

(4) The simulation results show that the accumulated water in the pipe can be cleaned from the bottom of the pipe by the oil flow. With the increase of oil phase inlet flow rate, the water carrying capacity of oil also increases. As the pipeline inclined angle increases from 10° to 40°, the water carrying capacity of oil firstly increases and then decreases.

Author Contributions: Data analysis, T.Z., B.C.; writing—original draft preparation, T.Z., B.C.; writing—review and editing, T.Z., B.C.; designed the research framework, K.S., W.C. All authors have read and agreed to the published version of the manuscript.

Funding: This research received no external funding.

Conflicts of Interest: The authors declare no conflict of interest.

References

- Shi, H.; Wang, L.; Luan, L. Aseismic design of Lanzhou–Chengdu–Chongqing oil product pipeline. *Oil Gas Storage Transp.* **2009**, *28*, 57–93.

2. Zhou, L. Construction experiences of Lanzhou-Chengdu-Chongqing transportation oil pipeline. *Pipeline Tech. Equip.* **2006**, *3*, 1–2. [[CrossRef](#)]
3. Wang, R.; Liu, X.; Wang, D. Discussion on formation mechanism of landslide disaster and its prevention. *J. Jiangnan Pet. Univ. Staff Work.* **2015**, *28*, 41–43. [[CrossRef](#)]
4. Jin, Z. Corrosion failure analysis of a certain product oil pipeline. *Pet. Tubul. Goods Instrum.* **2015**, *1*, 54–58. [[CrossRef](#)]
5. Liu, G.; Hao, J.; Lu, X.; Chen, L.; Sui, B. Development of monitoring system carrying impurity of product oil and corrosion in oil pipeline. *Res. Explor. Lab.* **2017**, *36*, 59–63, 102. [[CrossRef](#)]
6. Li, T.; Fan, J.; Liang, Y.; Liu, Y. The numerical simulation of the water's motion states in oil pipeline. *J. Shandong Univ. Technol.* **2015**, *29*, 60–65. [[CrossRef](#)]
7. Liu, M.; Jiang, Y.; Han, S.; Lv, X.; Ren, A.; Liu, W.; Yan, B.; Chen, X. Internal corrosion cause analysis of a products pipeline before putting into operation. *Corros. Sci. Prot. Technol.* **2018**, *30*, 496–502. [[CrossRef](#)]
8. Xu, G.; Zhang, G.; Zhao, S. An experiment on dewatering for lower location of pipeline. *Oil Gas Storage Transp.* **2011**, *30*, 369–372.
9. Liu, E.; Li, W.; Cai, H.; Peng, S. Formation mechanism of trailing oil in product oil pipeline. *Processes* **2019**, *7*, 7. [[CrossRef](#)]
10. Song, X.; Xiong, K.; Zhu, J.; Yu, D. Influence of water carrying capacity of oil products on internal corrosion of pipelines. *Oil Gas Storage Transp.* **2015**, *34*, 834–838. [[CrossRef](#)]
11. Peng, S.; Chen, Q.; Zheng, C.; Liu, E. Analysis of particle deposition in a new-type rectifying plate system during shale gas extraction. *Energy Sci. Eng.* **2019**, *8*, 702–717. [[CrossRef](#)]
12. Zhang, P.; Zhang, J.; Li, W.; Jiang, H.; Gong, J. Research on oil-water displacement in upward inclined pipes. *Nat. Gas Oil* **2019**, *37*, 8–14. [[CrossRef](#)]
13. Su, Z.; Liu, E.; Xu, Y.; Xie, P.; Shang, C.; Zhu, Q. Flow field and noise characteristics of manifold in natural gas transportation station. *Oil Gas Sci. Technol.* **2019**, *74*, 70. [[CrossRef](#)]
14. Zhao, S.; Hao, Y. Study on numerical simulation of the wave characteristics at oil-water interface in upward inclined pipeline. *Chem. Equip. Technol.* **2014**, *35*, 10–13. [[CrossRef](#)]
15. Song, X.; Li, D.; Sun, X.; Mou, X.; Chen, Y.; Yang, Y. Numerical modeling of the critical pipeline inclination for the elimination of the water accumulation on the pipe floor in oil-water fluid. *Petroleum* **2020**. [[CrossRef](#)]
16. Song, X.; Yang, Y.; Zhang, T.; Xiong, K.; Wang, Z. Studies on water carrying of diesel oil in upward inclined pipes with different inclined angle. *J. Pet. Sci. Eng.* **2017**, *157*, 780–792. [[CrossRef](#)]
17. Xu, G.; Cai, L.; Ullmann, A.; Brauner, N. Experiments and simulation of water displacement from lower sections of oil pipelines. *J. Pet. Sci. Eng.* **2016**, *147*, 829–842. [[CrossRef](#)]
18. Magnini, M.; Ullmann, A.; Brauner, N.; Thome, J. Numerical study of water displacement from the elbow of an inclined oil pipeline. *J. Pet. Sci. Eng.* **2018**, *166*, 1000–1017. [[CrossRef](#)]
19. Zhu, S.; Mou, X.; Li, W.; Song, X.; Gu, L. An experimental study on the flow patterns of oil-water two-phase flow in an upwardly inclined pipe. *J. Southwest Pet. Univ.* **2019**, *41*, 144–151. [[CrossRef](#)]
20. Wen, S.; Zhang, T.; Zhang, Q. Phase distribution identification method for oil-water two-phase flow in updip. *Oil Gas Storage Transp.* **2019**, *38*, 1022–1028. [[CrossRef](#)]
21. Gao, H.; Gu, H.; Guo, L. Numerical study of stratified oil–water two-phase turbulent flow in a horizontal tube. *Int. J. Heat Mass Transf.* **2003**, *46*, 749–754. [[CrossRef](#)]
22. Garmroodi, M.D.; Ahmadpour, A. Numerical simulation of stratified waxy crude oil and water flows across horizontal pipes in the presence of wall heating. *J. Pet. Sci. Eng.* **2020**, *193*, 107458. [[CrossRef](#)]
23. Xu, G.; Zhang, G.; Liu, G.; Zhang, X.; Zhang, Y. Distribution Model of Water Phase Interface in Oil Transportation Pipeline with Water. *Oil Gas Storage Transp.* **2010**, *29*, 821–826. [[CrossRef](#)]
24. Xu, G.; Zhang, G.; Brauner, N.; Ullmann, A.; Liu, G.; Zhang, X. Interface profile in oil-dragging-water pipeline system. *J. China Univ. Pet.* **2011**, *35*, 124–129. [[CrossRef](#)]
25. Zhang, H.; Lan, H.; Lin, N. A numerical simulation of water distribution associated with internal corrosion induced by water wetting in upward inclined oil pipes. *J. Pet. Sci. Eng.* **2019**, *173*, 351–361. [[CrossRef](#)]
26. Xu, G.; Zhang, G.; Zhao, S.; Wang, S. Analysis of characteristics of the oil purging water system in horizontal tube. *J. Southwest Pet. Univ.* **2011**, *33*, 173–177, 204. [[CrossRef](#)]
27. Wu, J.; Jiang, W.; Liu, Y.; He, Y.; Chen, J.; Qiao, L.; Wang, T. Study on hydrodynamic characteristics of oil-water annular flow in 90° elbow. *Chem. Eng. Res. Des.* **2020**, *153*, 443–451. [[CrossRef](#)]

28. Ersoy, G.; Sarica, C.; Al-Safran, E.; Zhang, H. Three-phase gas-oil-water flow in undulating pipeline. *J. Pet. Sci. Eng.* **2017**, *156*, 468–483. [[CrossRef](#)]
29. Zhang, T.; Chen, B.; Wen, S.; Song, X.; Zhang, Z. Numerical study on diesel oil carrying water behaviors in inclined pipeline based on large eddy simulation. *IEEE Access* **2019**, *7*, 123219–123230. [[CrossRef](#)]
30. Lafmejani, S.S.; Olesen, A.C.; Kær, S.K. VOF modelling of gas–liquid flow in PEM water electrolysis cell micro-channels. *Int. J. Hydrogen Energy* **2017**, *42*, 16333–16344. [[CrossRef](#)]
31. Labourasse, E.; Lacanette, D.; Toutant, A.; Lubin, P.; Vincent, S.; Lebaigue, O.; Caltagirone, J.P.; Sagaut, P. Towards large eddy simulation of isothermal two-phase flows: Governing equations and a priori tests. *Int. J. Multiphase Flow* **2007**, *33*, 1–39. [[CrossRef](#)]
32. Wang, C.; Zheng, X.; Li, L.; Ai, Z. Influence of Y^+ on the calculation of submarine flow field characteristics of LES. *J. Huazhong Univ. Sci. Technol.* **2015**, *43*, 79–83. [[CrossRef](#)]
33. Lodh, B.; Das, A.; Singh, N. Investigation of Turbulence for Wind Flow over a Surface Mounted Cube using Wall Y^+ Approach. *Indian J. Sci. Technol.* **2017**, *10*, 1–11. [[CrossRef](#)]



© 2020 by the authors. Licensee MDPI, Basel, Switzerland. This article is an open access article distributed under the terms and conditions of the Creative Commons Attribution (CC BY) license (<http://creativecommons.org/licenses/by/4.0/>).